ATMOSPHERIC SCIENCE

Global reduction in ship-tracks from sulfur regulations for shipping fuel

Tianle Yuan[1,2]*, Hua Song[2,3], Robert Wood[4], Chenxi Wang[1,2], Lazaros Oreopoulos[2], Steven E. Platnick[2], Sophia von Hippel[5], Kerry Meyer[2], Siobhan Light[6], Eric Wilcox[7,8]

Ship-tracks are produced by ship-emitted aerosols interacting with low clouds. Here, we apply deep learning models on satellite data to produce the first global climatology map of ship-tracks. We show that ship-tracks are at the nexus of cloud physics, maritime shipping, and fuel regulation. Our map captures major shipping lanes while missing others because of background conditions. Ship-track frequency is more than 10 times higher than a previous survey, and its interannual fluctuations reflect variations in cross-ocean trade, shipping activity, and fuel regulations. Fuel regulation can alter both detected frequency and shipping routes due to cost. The 2020 fuel regulation, together with the coronavirus disease 2019 pandemic, reduced ship-track frequency to its lowest level in recent decades across the globe and may have ushered in an era of low frequency. The regulation reduces the aerosol indirect forcing from ship emissions by 46% or between 0.02 and 0.27 W m^{-2} given its current estimates.

INTRODUCTION

Ship-tracks were first observed in early weather satellites as "anomalous cloud lines" (*1*) more than 55 years ago. They appear as quasi-linear tracks in marine low cloud fields (Fig. 1). Detection of ship-tracks in satellite data relies on a reflectance contrast between background and ship-track clouds (Fig. 1). The existence and detection of the contrast depend on various factors such as the wavelength of the observation and the background properties of cloud and aerosols, tiny suspended airborne particles (*2*–*5*). Hence, although ship emissions can affect low clouds by increasing aerosol concentrations, not all of them produce detectable ship-tracks. Ship-emitted aerosols produce ship-tracks by increasing the concentration of droplets in marine low clouds, which makes them appear brighter (*6*, *7*), the so-called aerosol indirect effects. Aerosol indirect effects act as a radiative forcing to Earth's climate by modifying cloud reflectance and amount and thus affecting Earth's energy balance (*8*, *9*). The aerosol indirect forcing partially counterbalances the radiative forcing caused by greenhouse gases. Existing estimates of aerosol indirect forcing from ship-emitted aerosols range from −0.06 to −0.6W m^{-2} (*10*–*15*). In addition to contributing to aerosol indirect forcing, ship-tracks have also been studied to understand aerosol indirect effects in general because they are idealized laboratories where aerosol effects can be clearly separated from effects of meteorology and other factors (*16*). Aerosol indirect forcing as a whole is the leading source of uncertainty in our estimate of various anthropogenic forcing components, and its magnitude has substantial implications for Earth's climate sensitivity (*9*, *17*). A strongly negative aerosol indirect forcing implies a climate that is highly sensitive to forcing by greenhouse gases as it makes the observed climate change the outcome of a small net positive forcing. In addition, ship-tracks can be viewed as inadvertent cloud brightening geoengineering experiments whose better understanding is necessary to consider deliberate experiments (*4*, *15*, *18*).

Despite the research interest in ship-tracks, only a single 1-year global survey has been carried out so far (*19*). It rejects more than 99% of observations because of data selection criteria (*19*). The lack

[1]Joint Center for Earth Systems Technology, University of Maryland, Baltimore County, Baltimore, MD, USA. [2]Sciences and Exploration Directorate, Goddard Space Flight Center, Greenbelt, MD, USA. [3]SSAI Inc., Lanham, MD, USA. [4]Department of Atmospheric Sciences, University of Washington, Seattle, WA, USA. [5]University of Arizona, Tucson, AZ, USA. [6]University of Maryland, College Park, MD, USA. [7]Desert Research Institute, Reno, NV, USA. [8]Interdisciplinary Program in Atmospheric Sciences, University of Nevada, Reno, Reno, NV, USA.
*Corresponding author. Email: tianle.yuan@nasa.gov

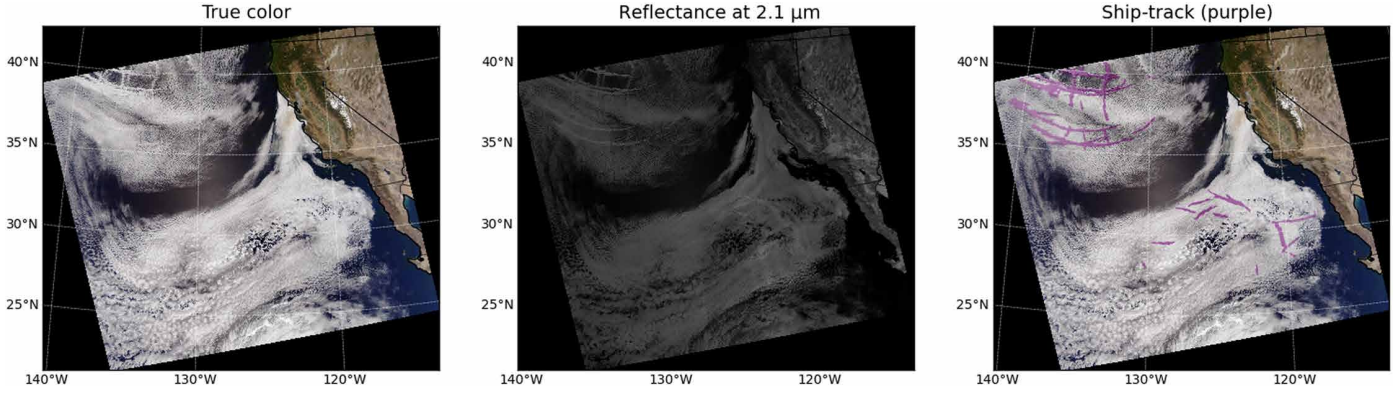

Fig. 1. Examples of ship-tracks detected by the model. An example MODIS granule off the west coast of North America. (**Left**) True color image. (**Middle**) Reflectance (2.1 μm). (**Right**) Detected ship-track mask overlaying on the true color image. Data (2.1 μm) are better at picking out ship-tracks that are not visible in the true color image.

of comprehensive global sampling of ship-tracks hinders the studies of aerosol indirect effects and geoengineering despite important progress made by analyzing manually labeled samples (*16*, *20*–*24*). Here, we combine deep learning models and global satellite observations to automatically identify ship-tracks at unprecedented scales in NASA's Aqua MODerate resolution Imaging Spectroradiometer (MODIS) daytime data. We show that large-scale sampling of ship-tracks can not only benefit aerosol indirect effect studies but also reveal unexpected connections among fuel regulation, shipping activity, and ship-tracks. The new dataset will improve progress toward understanding aerosol indirect effects in, and cloud brightening of, marine low clouds.

We train two independent deep neural network models on manually labeled ship-track samples using MODIS 2.1-μm data as input (Fig. 1) (*3*). We chose these two models from a pool of candidate models on the basis of their performance and ensemble-averaged their results to take advantage of their respective strengths. The ensemble average exhibits better performance than individual model results and generalizes well on test data that are independent of the training data. Details about model performance and validation can be found in Materials and Methods. The two trained models are then applied to Aqua MODIS data between 2003 and 2020.

RESULTS

Figure 2 shows the first global climatological map of ship-track density at 1° resolution. It is the result of processing 0.5 petabytes of data extending from 2003 to 2020. The density is calculated as the number of ship-track pixels divided by the total number of low cloud pixels, i.e., it is the fraction of low clouds belonging to ship-tracks. Low clouds are defined as clouds with top pressure higher than 680 hPa. Overlaid on the ship-track density are emissions of SO_2 from the global shipping industry (*25*) and MODIS annual mean low cloud fraction during the same period. The pattern of ship-track

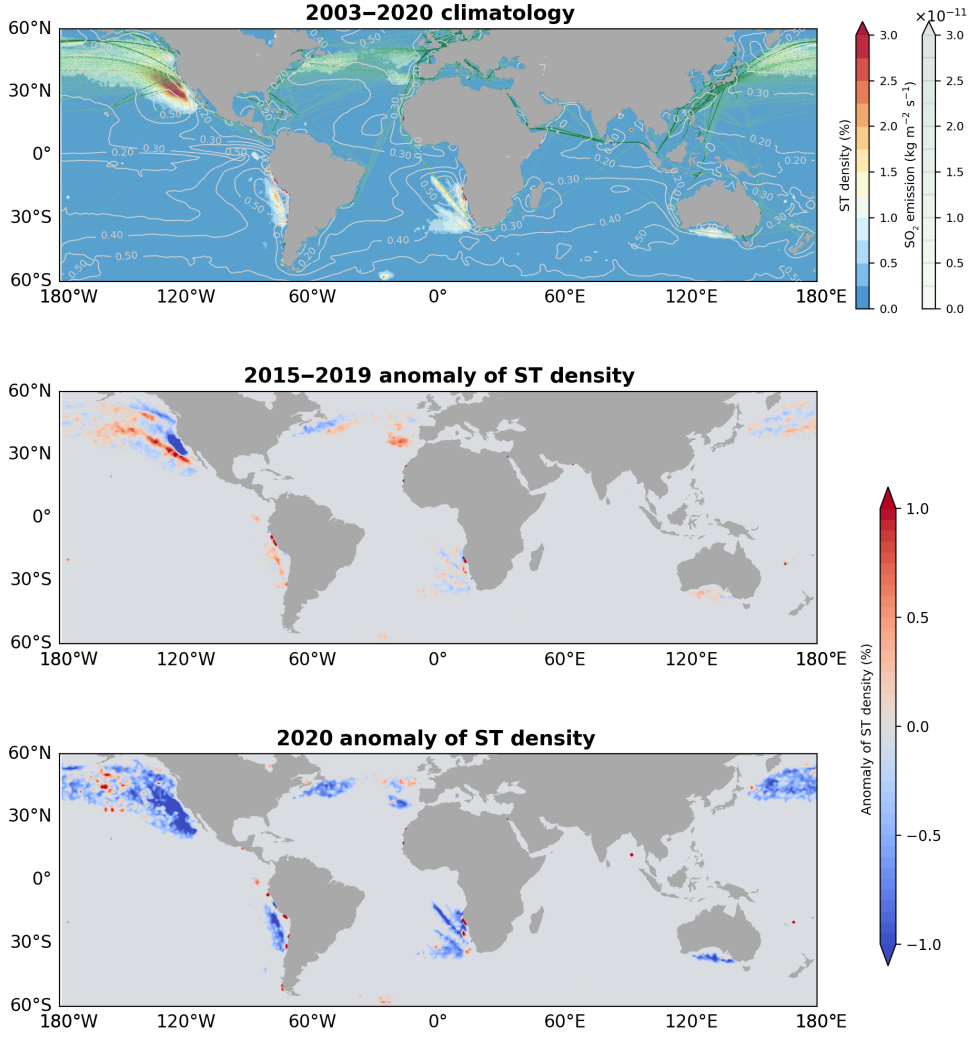

Fig. 2. Global climatology maps and anomalies for two periods. (**Top**) Climatological ship-track (ST) density map using data between 2003 and 2020. The gray contour lines show climatology of MODIS low cloud fraction. Green lines are for climatology of ship SO_2 emission data. The color maps are for ship-track density. (**Middle** and **bottom**) Ship-track density anomaly, relative to climatology, maps for four periods: 2015 to 2019 and 2020. The periods are chosen on the basis of fuel regulation standards. Anomaly maps for the other two periods of 2003 to 2009 and 2010 to 2014 can be found in the Supplementary Materials.

density generally follows that of ship SO_2 emissions, a proxy for shipping routes, in major maritime shipping lanes in the North and Southeast Pacific, in the Southeast Atlantic, in the North Atlantic, and to the south of Australia. The alignment between shipping routes and detected ship-track density varies with region. For example, the two are closely aligned in the Southeast Atlantic and Pacific and to the south of Australia, while in the Northern Pacific, especially near the west coast of North America, ship-track density appears much more spread out than the sharply defined shipping lines. This reflects the underlying alignment, or lack thereof, between prevailing winds and the direction of shipping lanes (*26*, *27*) and the steadiness of the circulation among other factors. Even when shipping lanes align directionally with detected ship-tracks, there is a consistent shift in location between the two. This is best observed in the Southeast Atlantic and near the Aleutian Islands, where the well-defined ship-track lanes are displaced by about one grid cell (1° in resolution) from the emission lines. This most likely reflects the horizontal expansion of ship-tracks with time as they are advected away from their initial formation. Because the number of ship-track pixels increases with expansion, a peak density is expected downwind of the initial formation. The magnitude of shift in the Southeast Atlantic and around Aleutian Islands is quite similar, suggesting similar underlying physics. The shift between emission and peak track density is also apparent for shipping routes with no well-defined lanes such as those off the California coast. Here, the detected ship-tracks form a blob instead of distinct lines downwind of shipping lines, and their magnitude of shift is larger. The absence of ship-tracks in other regions, e.g., the Tropics, can be explained by unfavorable background cloud and aerosol properties (see the Supplementary Materials).

An unexpected hot spot of apparent ship-tracks is found in the Southern Ocean around the South Sandwich Islands where hardly any marine traffic exists. Manual inspection shows that these tracks result from natural volcanic SO_2 plumes, which turn into sulfate aerosol plumes modifying cloud properties. Their interaction with clouds and signature in satellite data are almost identical to those of ship-tracks but at larger scales (*28*, *29*). The agreement between known shipping lanes and detected ship-track density and the independent detection of unexpected volcano tracks are further testaments of the robustness of our method.

Globally, ship-tracks are detected in about 0.3% of marine low clouds at the Aqua MODIS overpass time. Despite the low global value, our ship-track density represents an increase of more than an order of magnitude compared to the sole previous global survey (*19*). The overall low percentage is due to the lack of ship-tracks in the deep Tropics and the fact that ships follow narrow shipping lanes (see shipping emission in Fig. 2), leaving most ocean surface free of traffic by large ships. Our global figure represents only a lower bound on the percent of low clouds being affected by ship-emitted aerosols because many impacts are not in the form of ship-tracks (*14*) and explains why large-scale radiative impacts of ship emissions are hard to detect in observations (*30*). Locally, in as much as 2 to 3% of the low clouds are ship-tracks detected, mainly in subtropical regions dominated by stratocumulus clouds. For example, annual mean ship-track density can exceed 3% in local maxima near the west coast of North America.

In addition to explicitly forming detectable ship-tracks, ship-emitted aerosols can also affect clouds in other ways. For example, as ship-tracks evolve and dissipate with time, they appear as cloudy pixels that are hard to separate from background clouds (*2*, *15*, *22*). Also, when background clouds are polluted, detection of ship-tracks becomes less likely, although ship-emitted aerosols still affect clouds. This is best illustrated using the Southeast Atlantic shipping lane as an example. Few ship-tracks are detected (see Fig. 2 and fig. S4) in the segment between 0°S and 10°S. Nonetheless, a recent study shows that ship-emitted aerosols have strong effects on cloud droplet size and radiative energy balance for this segment during the same season (*27*). Again, detection of ship-tracks is not a necessary condition for ship-emitted aerosols to be modifying cloud properties (*24*).

Fuel regulations and economic activities are direct drivers of ship-track density. To illustrate the impact of both factors, we focus on the Northeast Pacific region because it has the highest ship-track density, and there is an Emission Control Area (ECA) under fuel regulations by the International Maritime Organization (outlined in fig. S1) (*31*). ECAs are established to control the fuel sulfur content of ships that travel inside them. In this ECA, no sulfur standard was implemented before 2005, but fuel sulfur content was limited to 1% in 2010 and 0.1% in 2015. Outside of ECAs, fuel sulfur content was uniformly reduced to 0.5% globally in 2020 from 3.5% (*31*).

The strict 2015 fuel standard inside the ECA has clear impacts on both ship-track density within the ECA and pattern of shipping routes outside of it. Within the ECA, detected ship-track density fell by nearly 70% after 2015. On the other hand, the effect of the 2010 standard was much more muted by comparison, given the small difference between 2010 to 2014 and 2005 to 2009 means. The strong reduction of ship-track density after 2015 is due not only to reduced emissions of sulfur (*32*), which produces a smaller droplet number concentration perturbation and therefore reduces the likelihood of detection, but also to changes in shipping routes (*24*, *33*). There are two major shipping routes within this region as seen in Fig. 2, the northern route connecting Asia to ports of Seattle and Vancouver and the southern route to various ports in California, Mexico, and South America. Both routes experience a clear southward shift starting in 2015. We believe that both shifts are purposely made by shipping companies to reduce ships' travel time within the ECA (*33*). While the southward shift of the northern route increases the total distance traveled by cruising along the ECA edge to a point that is closest to destination ports and then sailing straight toward them, the time spent within ECA is reduced. The fuel regulation provides enough incentive for shipping companies to make this shift so that ships travel less inside the ECA (*33*). The change in the southern route is even more marked. The 2015 fuel policy not only drove ships outside the ECA but also makes the shipping route more "contracted." Before 2015, detected ship-tracks in this area are more "spread out," forming a blob of high ship-track density. After 2015, ships are much more likely to travel along a narrower corridor. The contraction is apparent as a line of positive density anomaly straddled by strong negative anomalies on both sides.

The impact of the 2020 global fuel standard, representing an 86% reduction of fuel sulfur content outside of ECAs, is the most notable globally. It causes the ship-track density to reach a global minimum in 2020 for both this region and across the globe (Figs. 2 and 3). Ship-track density experiences strong reductions in every detected major shipping lane compared to climatology and reaches record lows in the nearly 20-year data record. Except the trans-Pacific and trans–North Atlantic shipping lanes, other shipping lanes are not discernible any longer (fig. S2). Annual mean ship-track

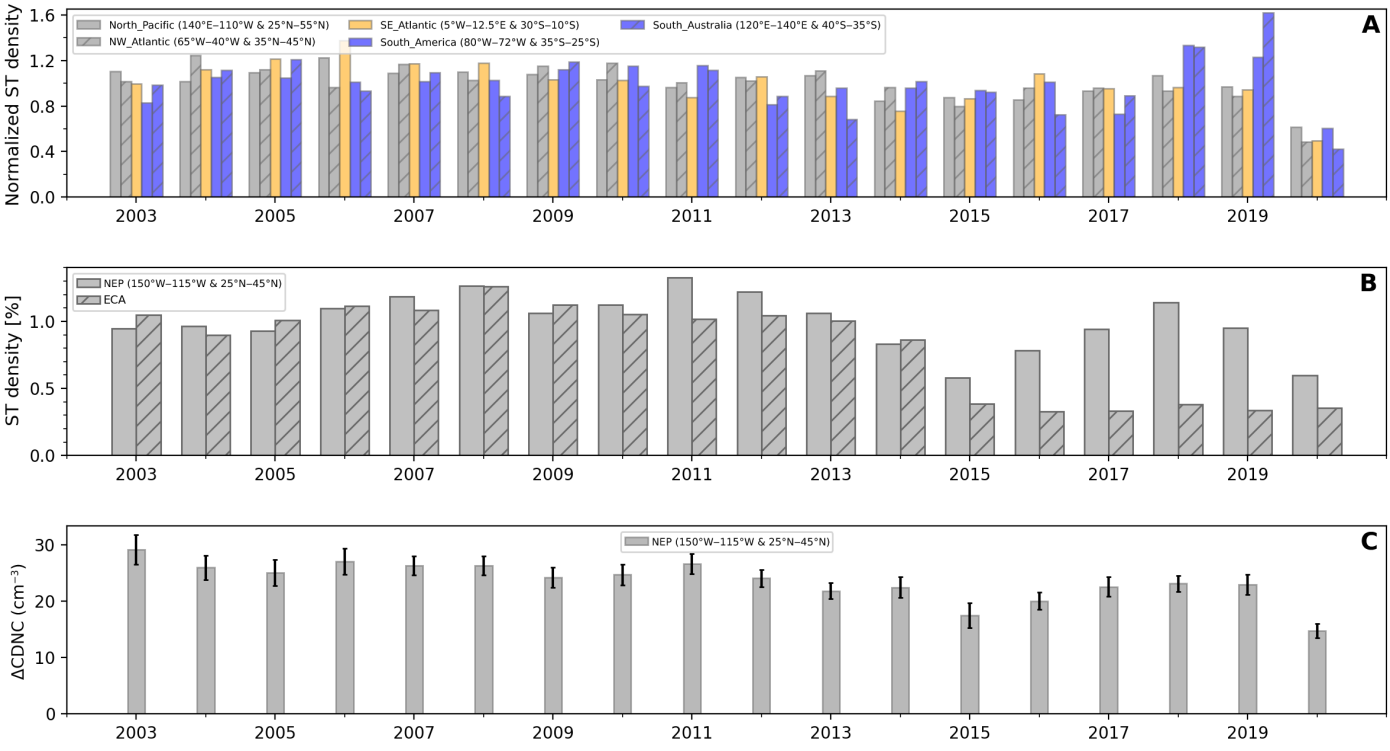

Fig. 3. Time series of ship-track density and N_d changes. (**A**) Normalized time series of ship-track density for five major shipping lanes. Each of the annual mean data is divided by this region's climatology to make it easier to compare different regions. (**B**) Time series in the Northeast Pacific (NEP) and ECA in particular. Data are not normalized for (B). (**C**) Time series for ship-induced N_d change for clean background clouds. ΔCDNC, difference of cloud droplet number concentration.

density decreases by 50% or more in five major shipping lanes compared to the climatological mean. The decline is even steeper if compared to 2019. Both fuel regulations and temporarily reduced international shipping activity due to the coronavirus disease 2019 (COVID-19) pandemic have contributed to this global reduction (*31*, *34*), although the latter factor is likely a minor contributor. Ship-based automatic identification system (AIS) data show a 1.4% decrease in global shipping traffic and do not suggest such a strong reduction in annual shipping traffic due to COVID-19 (*34*), and 7 months of 2021 data show that detected ship-tracks remain at record-low levels and comparable to 2020, although the reduction caused by COVID-19 only lasted a few months in 2020. This suggests that fuel regulation plays the most dominant role. The global 2020 fuel standard is likely a watershed moment that will permanently reduce the population of detectable ship-tracks.

Fluctuations in international trade and economic activity can also leave fingerprints on detected ship-track density. To illustrate this, we select a region in the Northeast Pacific to capture trans-Pacific shipping activity between Asia and the Americas. The general upward trend of shipping activity between 2003 and 2013 is reflected in the time series of ship-track density (*35*). The upward trend has a noticeable dip in 2009 to 2010, coinciding with the aftereffect of the financial crisis of 2008. However, a stronger decrease occurs between 2014 and 2016, likely caused by a strong slowdown in the Chinese economy (*35*). The ship-track density bounces back quickly and reaches another peak in 2018, from where it starts to decrease slightly again, possibly reflecting the trade tension at that time. The

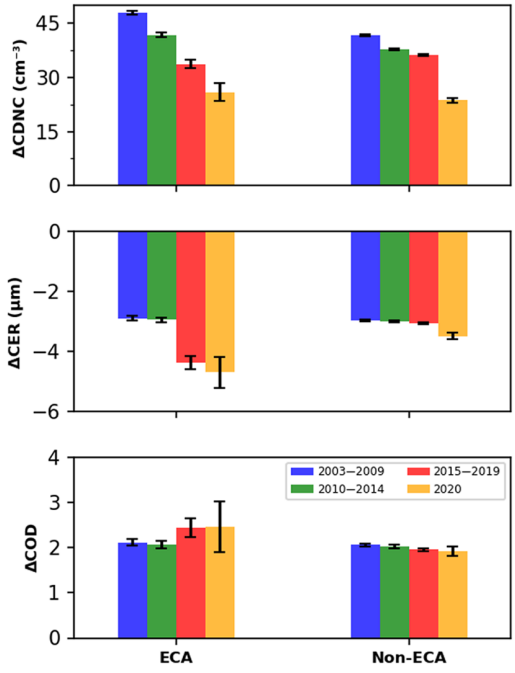

Fig. 4. Changes in cloud properties in ship-tracks. Difference of cloud droplet number concentration, cloud effective radius (CER), and cloud optical depth between ship-track and background for four regions in the Northeast Pacific (see fig. S1 for ECA and non-ECA region shapes).

density in 2020 drops precipitously because of the new fuel standard and COVID-19 (*34*).

Changes in fuel regulation offer opportunities to examine how cloud microphysical and optical properties respond to different magnitudes of aerosol perturbations inside ship-tracks. Figure 4 shows perturbations in cloud properties during four periods of different fuel standards. The perturbations are taken as differences in cloud droplet number concentration, N_d, and cloud effective radius, R_e, between ship-track and background pixels using the MODIS cloud product (see Materials and Methods) (*36*). We separate the Northeast Pacific into two regions: ECA and its vicinity as non-ECA. Within the ECA region, N_d perturbations, ΔN_d, show a monotonic decrease with increasingly stricter fuel standards, reflecting smaller aerosol perturbations. ΔN_d decreases from 47 cm^{-3} during 2003 to 2009 to about 31 cm^{-3} during 2015 to 2019. The decrease is statistically significant above the 95% confidence level. Unexpectedly, the R_e perturbation increases with decreasing N_d perturbation. This is mostly because the background cloud properties have also changed. Clouds of cleaner background are required for ship-tracks to be detected as the amount of emitted aerosols decreases. With lower background N_d, the background droplet size is larger. This is in contrast to the neighboring non-ECA area, where neither quantity has a strong trend, except in 2020 when the new global fuel standard takes effect. Cloud optical depth (COD) difference between ship-tracks and the background is insensitive to fuel regulations (see Fig. 4 and Materials and Methods). The contrast between ECA and non-ECA regions highlights the impact of the fuel regulation on ship-tracks and the importance of the background clouds.

We estimate the overall impact of the 2020 fuel standard on global ship-emitted aerosols in the context of aerosol indirect effects by examining the droplet number difference between ship-track and background clouds (see Materials and Methods). We select only clean background clouds with a droplet number concentration between 10 and 20 cm^{-3} for two reasons: First, they occur frequently

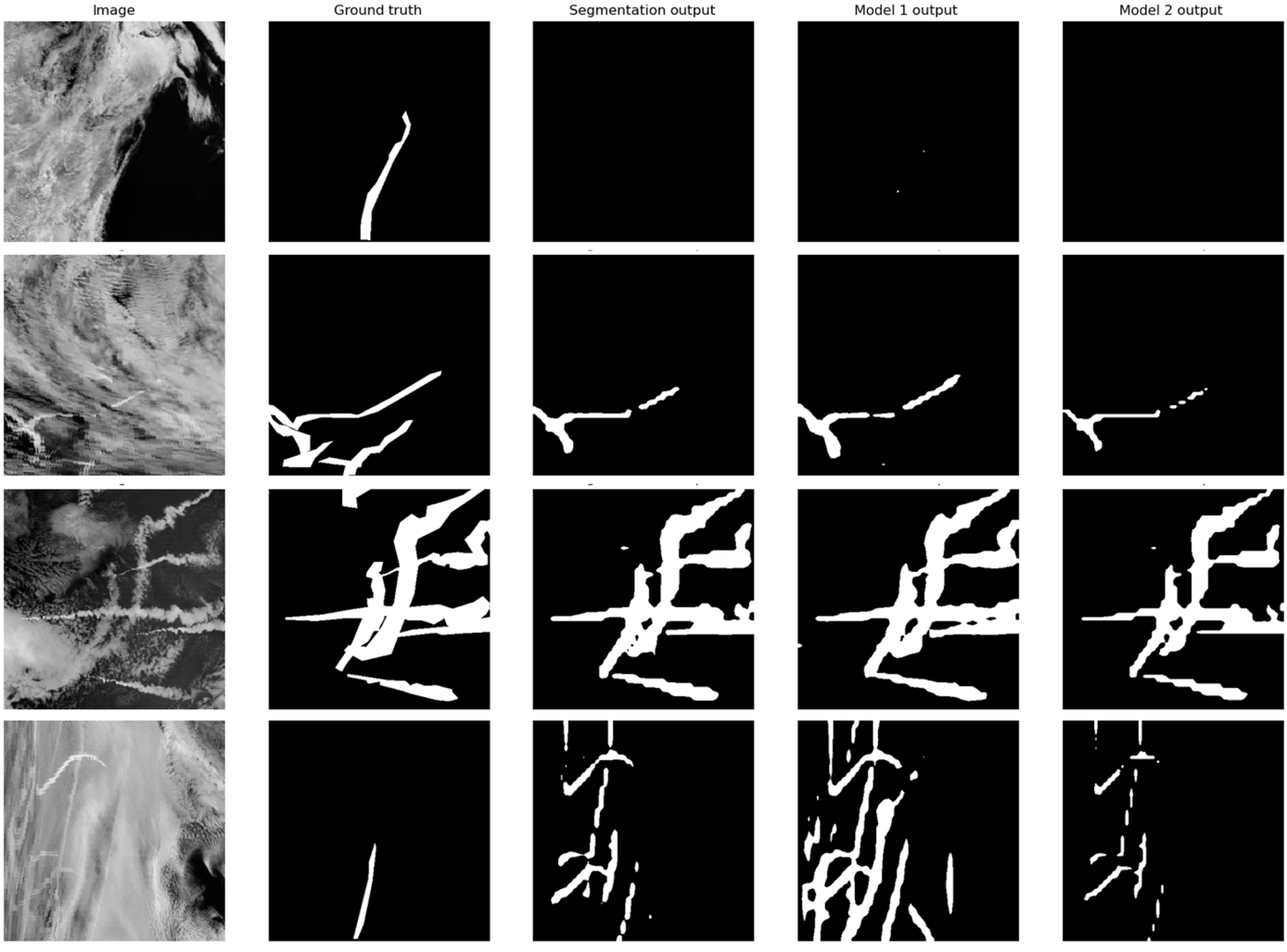

Fig. 5. Examples of model-detecting ship tracks. Four kinds of examples: (left) MODIS 2.1-μm images, (second to the left) manually labeled ship-track masks (white pixels), (middle) ship-track masks from an ensemble of models, and (right two) ship-track masks from two models. In the first example, the manual ship-track label is a false positive. In the second example, the models pick out most manual labels and leave out the questionable ones. Model and manual labels agree well in the third, quite complex example. In the last example, the labeler clearly missed many true positives, while the models correctly detected them. Most training and test samples fall into the second and third kinds.

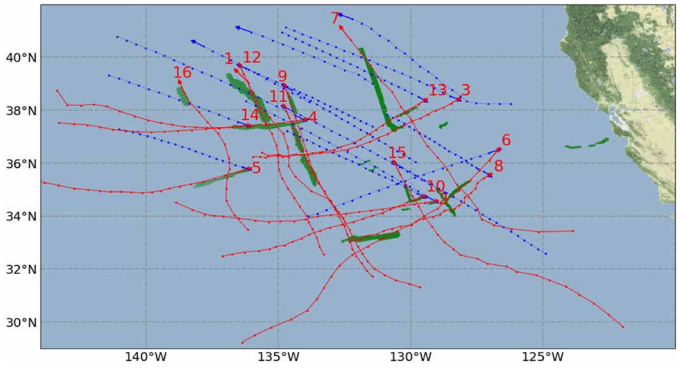

Fig. 6. An example of predicted tracks based on wind and AIS data, together with detected ship-track masks from our algorithm. We picked ships (indicated by numbers) whose predicted tracks matched with ship-track masks. Most match really well with ship number 7 slightly off, which could be attributed to imperfection in wind field or trajectory model.

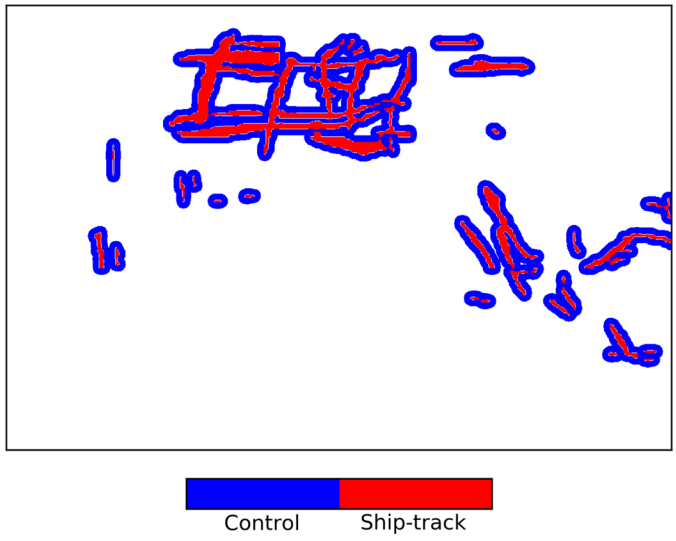

Fig. 7. Detected ship-track pixels and their background pixels for an Aqua granule taken at 2155 UTC on 15 July 2018. The width of the background (blue color in the figure) is 20 pixels.

in the ship-track database; second, they are more likely under an aerosol-limited condition, and thus, a high percentage of ship-emitted aerosols will activate into droplets, which makes changes in droplet number concentration more sensitive to changes in emitted aerosols. We use data from the Northeast Pacific given its abundant ship-track samples. Figure 3C shows a time series of droplet number concentration increase inside ship-tracks. The concentration decreases from a climatological mean of 27 to 17 cm^{-3} in 2020 or translates to an estimated 46% decrease in ship-emitted aerosols and associated forcing. If we simply scale aerosol emission decrease with indirect forcing due to ship emissions and ignore aerosol effects on cloud fraction, the 2020 fuel regulation would constitute a positive forcing between 0.02 and 0.27 W m^{-2} (see Materials and Methods for details and assumptions).

DISCUSSION

The first comprehensive survey of global ship-tracks reveals interesting connections between cloud physics, maritime shipping activity, and fuel regulation. Our ship-track database can find more applications in other research areas in the future. For example, the atmospheric chemistry and physics processes taking place between the emission of gases and the formation and detection of ship-tracks can be explored to understand the expansion and detection of ship-tracks. Analysis of ship-tracks may be used for fuel regulation compliance in open oceans. Given the order of magnitude increase in detected ship-tracks (*19*), observation-based estimate of radiative forcing from ship emissions needs to be reassessed. In addition, explicitly detected ship-tracks only represent a lower bound on the ship-emitted aerosols' impact on maritime clouds. For example, a rough estimate based on our ship-track density and previous studies (*19*, *27*) would put such forcing on the order of −1 W m^{-2} or more for major ship-track lanes. More in-depth analysis of the aerosol-cloud interactions using comprehensive ship-track data will benefit the understanding of aerosol indirect effects on low clouds in general since such effects are known to be nonlinear and sensitive to environmental conditions (*20*–*24*, *37*). Such studies will also help assess the effectiveness and impact of deliberate marine cloud brightening as a geoengineering option. The impact of fuel regulations shown here is a demonstration of both significant human impacts on the marine clouds and our ability to change them with appropriate policies/methods. The evolving impact of the regime changing 2020 fuel standard warrants close monitoring in the coming years given its potential radiative forcing.

MATERIALS AND METHODS

Ship-track detection and validation

We use the architecture provided by Ronneberger *et al.* (*38*) to train the model, similar to the nighttime model that we developed before (*26*). We carry out a set of experiments to adjust hyperparameters such as the number of downsampling blocks and the learning rate. We train the model with different loss functions such as L2 loss, focal loss, and cross-entropy (*38*). L2 loss is mean square error loss. We then pick two models that have complementary strengths as our final ensemble. They use L2 loss and focal loss, respectively. The number of layers in the down and up branches are both five. The number of filters increases from 16 to 256. A tanh activation function is used for the output layer. We trained both models for 100 epochs. The output of each model at each pixel can be viewed as a likelihood of that pixel being a ship-track pixel. We simply average the two models' output as the final output and use 0.3 as the threshold for binary classification for each pixel. A few examples are given in Fig. 5. The train/validation split is 0.8/0.2.

When tested on a validation dataset, i.e., labeled samples never seen by the models, our ensemble model achieves an F_1 score of 0.81, precision of 0.87, and recall of 0.77 on test data. Precision is defined as $p = \frac{\{\text{Predicted positives}\} \cap \{\text{Labeled positives}\}}{\{\text{Predicted positives}\}}$. Recall is defined as $r = \frac{\{\text{Predicted positives}\} \cap \{\text{Labeled positives}\}}{\{\text{Labeled positives}\}}$. F_1 score balances the precision and recall and is defined as

$$F_1 = 2 \times \frac{p \times r}{p + r}$$

In addition to validate model outputs on test manual labels, we also have a qualitative validation method to independently test our model output against never-seen samples using a trajectory model. This is because the ground truth for ship-tracks is hard to find for satellite data–based detection because in situ observations are extremely limited. We can only rely on human inspection of the original reflectance, which is still not direct validation (*39*). We use AIS and Modern-Era Retrospective Analysis for Research and Applications, version 2 (MERRA-2) reanalysis data to validate our detections. AIS data report real-time ship data such as location and speed every 6 min and are publicly available for ships around U.S. coastal regions. We developed a forward trajectory model to facilitate validating ship-track detection. The forward trajectory model uses MERRA-2 (*40*) near-surface wind to advect ship emission based on AIS data. The 1-hourly averaged 50-m U and V wind components from MERRA-2 high-spatial resolution (0.625° × 0.5°) data are used. The 6-min AIS ship location data are downsampled to the half-hourly. Each ship releases a virtual emission parcel at every time step, and the forward trajectory model predicts their locations at satellite passing time. We then obtain an expected ship emission track at the MODIS overpassing time by connecting predicted locations of each virtual parcel. These expected tracks are compared with the actual detected ship-tracks for validation.

Figure 6 gives an example where blue lines show actual trajectories of 16 vessels between 0000 and 2200 UTC (Coordinated Universal Time), 17 July 2018. Red lines are predicted ship emission tracks at 2130 UTC using the forward trajectory model. Detected ship-track masks by our algorithms are shown in green. The predicted tracks by forward model match well with detected ship-track masks by our algorithms. We note that ship-track masks can be broken because of broken low clouds and/or overlapping high clouds. Ship number 7's predicted track is slightly off from the actual ship-track mask, possibly reflecting imperfect wind fields or forward model. Overall, the match-up provides an excellent qualitative validation for our detection model.

Analysis of aerosol indirect effects using ship-tracks

For each detected ship-track, we automatically find background pixels surrounding it whose width is 20 pixels on both sides as shown in Fig. 7. Each granule, approximately 2030 × 1350, is then broken into small blocks of size 128 × 128. Within each block, we calculate mean values of cloud variables such as droplet effective radius, COD, and cloud droplet number concentration for the background and ship-track pixels. The difference between background and ship-track pixels' means is taken as the impact caused by ship-emitted aerosols. Aggregating values from many such blocks leads to the mean values and 95% uncertainty ranges reported in Fig. 4.

Estimating aerosol indirect forcing due to regulation

First, we have $\frac{\Delta \mathrm{COD}}{\mathrm{COD}} = \frac{\Delta \mathrm{LWP}}{\mathrm{LWP}} - \frac{\Delta R_e}{R_e}$, where LWP is liquid water path, and R_e is cloud effective radius (*21*). ΔCOD is thus usually proportional to background COD if the ratio is close to constant, which is mostly supported by our data (Fig. 4).

Without considering aerosol effects on cloud fractions, cloud albedo sensitivity to aerosols can be taken as the sum of the Twomey effect and aerosol-induced LWP changes

$$S = \frac{dA_c}{dN_d} = \frac{A_c(1-A_c)}{3N_d} \times \left(1 + \frac{5}{2}\frac{d\ln \mathrm{LWP}}{d\ln N_d}\right)$$

where S is the susceptibility of cloud albedo (A_c) to droplet number concentration (N_d) (*23*). Aerosol indirect forcing is therefore

$$\Delta \mathrm{SW}_{\mathrm{TOA}} = -\mathrm{SW}_{\mathrm{downwelling}} \times \mathrm{CF}_{\mathrm{liquid}} \times A_c \times$$

$$(1-A_c) \times \left(\frac{1}{3} + \frac{5}{6}\frac{d\ln \mathrm{LWP}}{d\ln N_d}\right) \times \Delta \ln N_d$$

We have $\Delta SW_{TOA} \sim \Delta \ln N_d$ and $\Delta \ln N_d$. To get $\Delta \ln N_d$,we target background clouds that are clean. Clean background clouds ensure that a high fraction of ship-emitted aerosols would activate into droplets, and the difference between ship-track and background clouds in N_d, i.e., ΔN_d, can therefore better capture the changes in the number of ship-emitted aerosols (*41*). We find these clean clouds in each year, and time series of ΔN_d for these clean clouds reflects the impact of fuel regulations on N_d (*32*). Once we estimate the impact of fuel regulations on ΔN_d using clean background clouds, we assume that the magnitude of change in underlying ship-emitted aerosols due to fuel regulation is the same for all ships and conditions on average. The ship emission change due to regulation should have no correlation with background cloud properties, which we believe is a reasonable assumption. We can thus obtain $\Delta \ln N_d$. From the literature, aerosol indirect forcing due to ship emissions is estimated to be −0.06 to −0.6 W m^{-2}, and therefore, forcing due to fuel regulation is 46% of that as shown in the text, i.e., 0.02 to 0.27 W m^{-2}, assuming that the LWP and cloud fraction responses are constant, although we have clear evidence of aerosol effects on cloud fraction (*42*).

For the region off the coast of California where the highest ship-track density is found, we estimate the order of magnitude of the aerosol indirect forcing due to ship emissions by comparing the low cloud coverage and ship-track densities of this region and that of the southeast Atlantic (*27*). They have similar cloud coverage, and the Californian region has higher ship-track density. The forcing estimated for the southeast Atlantic region is −1.9 to −2.2 W m^{-2} using bottom-up and top-down estimates, respectively. We think that it is on the same order of magnitude for the California region, i.e., 1 W m^{-2}.

SUPPLEMENTARY MATERIALS

Supplementary material for this article is available at https://science.org/doi/10.1126/sciadv.abn7988

REFERENCES AND NOTES

1. J. H. Conover, Anomalous cloud lines. *J. Atmos. Sci.* **23**, 778–785 (1966).
2. J. A. Coakley, P. A. Durkee, K. Nielsen, J. P. Taylor, S. Platnick, B. A. Albrecht, D. Babb, F.-L. Chang, W. R. Tahnk, C. S. Bretherton, P. V. Hobbs, The appearance and disappearance of ship tracks on large spatial scales. *J. Atmos. Sci.* **57**, 2765–2778 (2000).
3. S. Platnick, P. A. Durkee, K. Nielsen, J. P. Taylor, S. C. Tsay, M. D. King, R. J. Ferek, P. V. Hobbs, J. W. Rottman, The role of background cloud microphysics in the radiative formation of ship tracks. *J. Atmos. Sci.* **57**, 2607–2624 (2000).
4. H. Wang, P. J. Rasch, G. Feingold, Manipulating marine stratocumulus cloud amount and albedo: A process-modelling study of aerosol-cloud-precipitation interactions in response to injection of cloud condensation nuclei. *Atmos. Chem. Phys.* **11**, 4237–4249 (2011).
5. A. Possner, H. Wang, R. Wood, K. Caldeira, T. P. Ackerman, The efficacy of aerosol–cloud radiative perturbations from near-surface emissions in deep open-cell stratocumuli. *Atmos. Chem. Phys.* **18**, 17475–17488 (2018).
6. J. A. Coakley, R. L. Bernstein, P. A. Durkee, Effect of ship-stack effluents on cloud reflectivity. *Science* **237**, 1020–1022 (1987).
7. S. Twomey, The influence of pollution on the shortwave albedo of clouds. *J. Atmos. Sci.* **34**, 1149–1152 (1977).

8. J. H. Seinfeld, C. Bretherton, K. S. Carslaw, H. Coe, P. J. DeMott, E. J. Dunlea, G. Feingold, S. Ghan, A. B. Guenther, R. Kahn, I. Kraucunas, S. M. Kreidenweis, M. J. Molina, A. Nenes, J. E. Penner, K. A. Prather, V. Ramanathan, V. Ramaswamy, P. J. Rasch, A. R. Ravishankara, D. Rosenfeld, G. Stephens, R. Wood, Improving our fundamental understanding of the role of aerosol–cloud interactions in the climate system. *Proc. Natl. Acad. Sci. U.S.A.* **113**, 5781–5790 (2016).
9. N. Bellouin, J. Quaas, E. Gryspeerdt, S. Kinne, P. Stier, D. Watson-Parris, O. Boucher, K. S. Carslaw, M. Christensen, A.-L. Daniau, J.-L. Dufresne, G. Feingold, S. Fiedler, P. Forster, A. Gettelman, J. M. Haywood, U. Lohmann, F. Malavelle, T. Mauritsen, D. T. McCoy, G. Myhre, J. Mülmenstädt, D. Neubauer, A. Possner, M. Rugenstein, Y. Sato, M. Schulz, S. E. Schwartz, O. Sourdeval, T. Storelvmo, V. Toll, D. Winker, B. Stevens, Bounding global aerosol radiative forcing of climate change. *Rev. Geophys.* **58**, e2019RG000660 (2020).
10. K. Capaldo, J. J. Corbett, P. Kasibhatla, P. Fischbeck, S. N. Pandis, Effects of ship emissions on sulphur cycling and radiative climate forcing over the ocean. *Nature* **400**, 743–746 (1999).
11. A. Lauer, V. Eyring, J. Hendricks, P. Jöckel, U. Lohmann, Global model simulations of the impact of ocean-going ships on aerosols, clouds, and the radiation budget. *Atmos. Chem. Phys.* **7**, 5061–5079 (2007).
12. K. Peters, P. Stier, J. Quaas, H. Graßl, Aerosol indirect effects from shipping emissions: Sensitivity studies with the global aerosol-climate model ECHAM-HAM. *Atmos. Chem. Phys.* **12**, 5985–6007 (2012).
13. A. I. Partanen, A. Laakso, A. Schmidt, H. Kokkola, T. Kuokkanen, J.-P. Pietikäinen, V.-M. Kerminen, K. E. J. Lehtinen, L. Laakso, H. Korhonen, Climate and air quality trade-offs in altering ship fuel sulfur content. *Atmos. Chem. Phys.* **13**, 12059–12071 (2013).
14. V. Eyring, I. S. A. Isaksen, T. Berntsen, W. J. Collins, J. J. Corbett, O. Endresen, R. G. Grainger, J. Moldanova, H. Schlager, D. S. Stevenson, Transport impacts on atmosphere and climate: Shipping. *Atmos. Environ.* **44**, 4735–4771 (2010).
15. R. Wood, Assessing the potential efficacy of marine cloud brightening for cooling Earth using a simple heuristic model. *Atmos. Chem. Phys.* **21**, 14507–14533 (2021).
16. M. W. Christensen, A. Gettelman, J. Cermak, G. Dagan, M. Diamond, A. Douglas, G. Feingold, F. Glassmeier, T. Goren, D. P. Grosvenor, E. Gryspeerdt, R. Kahn, Z. Li, P.-L. Ma, F. Malavelle, I. L. McCoy, D. T. McCoy, G. McFarquhar, J. Mülmenstädt, S. Pal, A. Possner, A. Povey, J. Quaas, D. Rosenfeld, A. Schmidt, R. Schrödner, A. Sorooshian, P. Stier, V. Toll, D. Watson-Parris, R. Wood, M. Yang, T. Yuan, Opportunistic experiments to constrain aerosol effective radiative forcing. *Atmos. Chem. Phys.* **22**, 641–674 (2022).
17. T. F. Stocker, D. Qin, G.-K. Plattner, L. V. Alexander, S. K. Allen, N. L. Bindoff, F.-M. Bréon, J. A. Church, U. Cubasch, S. Emori, P. Forster, P. Friedlingstein, N. Gillett, J. M. Gregory, D. L. Hartmann, E. Jansen, B. Kirtman, R. Knutti, K. Krishna Kumar, P. Lemke, J. Marotzke, V. Masson-Delmotte, G. A. Meehl, I. I. Mokhov, S. Piao, V. Ramaswamy, D. Randall, M. Rhein, M. Rojas, C. Sabine, D. Shindell, L. D. Talley, D. G. Vaughan, S.-P. Xie, Technical summary. In *Climate Change 2013: The Physical Science Basis. Contribution of Working Group I to the Fifth Assessment Report of the Intergovernmental Panel on Climate Change*, T. F. Stocker, D. Qin, G.-K. Plattner, M. Tignor, S. K. Allen, J. Doschung, A. Nauels, Y. Xia, V. Bex, P. M. Midgley, Eds. (Cambridge University Press, 2013), pp. 33–115.
18. J. Latham, P. Rasch, C.-C. J. Chen, L. Kettles, A. Gadian, A. Gettelman, H. Morrison, K. Bower, T. Choularton, Global temperature stabilization via controlled albedo enhancement of low-level maritime clouds. *Pilos. Trans. R. Soc. A. Math. Phys. Eng. Sci.* **366**, 3969–3987 (2008).
19. M. Schreier, H. Mannstein, V. Eyring, H. Bovensmann, Global ship track distribution and radiative forcing from 1 year of AATSR data. *Geophys. Res. Lett.* **34**, L17814 (2007).
20. P. A. Durkee, R. E. Chartier, A. Brown, E. J. Trehubenko, S. D. Rogerson, C. Skupniewicz, K. E. Nielsen, S. Platnick, M. D. King, Composite ship track characteristics. *J. Atmos. Sci.* **57**, 2542–2553 (2000).
21. M. W. Christensen, G. L. Stephens, Microphysical and macrophysical responses of marine stratocumulus polluted by underlying ships: Evidence of cloud deepening. *J. Geophys. Res.* **116**, D03201 (2011).
22. Y.-C. Chen, M. W. Christensen, L. Xue, A. Sorooshian, G. L. Stephens, R. M. Rasmussen, J. H. Seinfeld, Occurrence of lower cloud albedo in ship tracks. *Atmos. Chem. Phys.* **12**, 8223–8235 (2012).
23. V. Toll, M. Christensen, J. Quaas, N. Bellouin, Weak average liquid-cloud-water response to anthropogenic aerosols. *Nature* **572**, 51–55 (2019).
24. E. Gryspeerdt, T. W. P. Smith, E. O'Keeffe, M. W. Christensen, F. W. Goldsworth, The Impact of ship emission controls recorded by cloud properties. *Geophys. Res. Lett.* **46**, 12547–12555 (2019).
25. M. Crippa, E. Solazzo, G. Huang, D. Guizzardi, E. Koffi, M. Muntean, C. Schieberle, R. Friedrich, G. Janssens-Maenhout, High resolution temporal profiles in the Emissions Database for Global Atmospheric Research. *Sci Data.* **7**, 121 (2020).
26. T. Yuan, C. Wang, H. Song, S. Platnick, K. Meyer, L. Oreopoulos, Automatically finding ship tracks to enable large-scale analysis of aerosol-cloud interactions. *Geophys. Res. Lett.* **46**, 7726–7733 (2019).
27. M. S. Diamond, H. M. Director, R. Eastman, A. Possner, R. Wood, Substantial cloud brightening from shipping in subtropical low clouds. *AGU Adv.* **1**, e2019AV000111 (2020).
28. S. Gasso, Satellite observations of the impact of weak volcanic activity on marine clouds. *J. Geophys. Res. Atmos.* 10.1029/2007JD009106 , (2008).
29. V. Toll, M. Christensen, S. Gassó, N. Bellouin, Volcano and ship tracks indicate excessive aerosol-induced cloud water increases in a climate model. *Geophys. Res. Lett.* **44**, 12,492–12,500 (2017).
30. K. Peters, J. Quaas, H. Graßl, A search for large-scale effects of ship emissions on clouds and radiation in satellite data. *J. Geophys. Res. Atmospheres.* **116**, D24205 (2011).
31. International Maritime Organization, *IMO 2020 Sulfur Oxide Emission Regulation* (2020); www.imo.org/en/MediaCentre/HotTopics/Pages/Sulphur-2020.aspx.
32. C. Yu, D. Pasternak, J. Lee, M. Yang, T. Bell, K. Bower, H. Wu, D. Liu, C. Reed, S. Bauguitte, S. Cliff, J. Trembath, H. Coe, J. D. Allan, Characterizing the particle composition and cloud condensation nuclei from shipping emission in Western Europe. *Environ. Sci. Technol.* **54**, 15604–15612 (2020).
33. K. Fagerholt, N. T. Gausel, J. G. Rakke, H. N. Psaraftis, Maritime routing and speed optimization with emission control areas. *Transport. Res. C Emerg. Technol.* **52**, 57–73 (2015).
34. D. March, K. Metcalfe, J. Tintoré, B. J. Godley, Tracking the global reduction of marine traffic during the COVID-19 pandemic. *Nat. Commun.* **12**, 2415 (2021).
35. S. Sirimanne, J. Hoffmann, R. Asariotis, G. Ayala, M. Assaf, C. Bacrot, H. Benamara, D. Chantrel, A. Cournoyer, M. Fugazza, P. Hansen, T. Kulaga, A. Premti, L. Rodriguez, B. Salo, K. Tahiri, H. Tokuda, P. Ugaz, F. Youssef, Review of maritime transport 2021, in *Review of Maritime Transport* (United Nations Publications, 2021); https://unctad.org/webflyer/review-maritime-transport-2021.
36. S. Platnick, K. G. Meyer, M. D. King, G. Wind, N. Amarasinghe, B. Marchant, G. T. Arnold, Z. Zhang, P. A. Hubanks, R. E. Holz, P. Yang, W. L. Ridgway, J. Riedi, The MODIS cloud optical and microphysical products: Collection 6 updates and examples from terra and aqua. *IEEE Trans. Geosci. Remote Sens.* **55**, 502–525 (2017).
37. M. Christensen, A. Gettelman, J. Cermak, G. Dagan, M. Diamond, A. Douglas, G. Feingold, F. Glassmeier, T. Goren, D. Grosvenor, E. Gryspeerdt, R. Kahn, Z. Li, P.-L. Ma, F. Malavelle, I. McCoy, D. McCoy, G. McFarquhar, J. Mülmenstädt, S. Pal, A. Possner, A. Povey, J. Quaas, D. Rosenfeld, A. Schmidt, R. Schrödner, A. Sorooshian, P. Stier, V. Toll, D. Watson-Parris, R. Wood, M. Yang, T. Yuan, Opportunistic experiments to constrain aerosol effective radiative forcing. *Atmos. Chemis. Phys.* **22**, 641–674 (2021).
38. O. Ronneberger, P. Fischer, T. Brox, U-Net: Convolutional networks for biomedical image segmentation. arXiv:1505.04597 [cs.CV] (18 May 2015).
39. J. A. Coakley, C. D. Walsh, Limits to the aerosol indirect radiative effect derived from observations of ship tracks. *J. Atmos. Sci.* **59**, 668–680 (2002).
40. R. Gelaro, W. McCarty, M. J. Suárez, R. Todling, A. Molod, L. Takacs, C. A. Randles, A. Darmenov, M. G. Bosilovich, R. Reichle, K. Wargan, L. Coy, R. Cullather, C. Draper, S. Akella, V. Buchard, A. Conaty, A. M. da Silva, W. Gu, G.-K. Kim, R. Koster, R. Lucchesi, D. Merkova, J. E. Nielsen, G. Partyka, S. Pawson, W. Putman, M. Rienecker, S. D. Schubert, M. Sienkiewicz, B. Zhao, The modern-era retrospective analysis for research and applications, Version 2 (MERRA-2). *J. Climate* **30**, 5419–5454 (2017).
41. V. A. Karydis, S. L. Capps, A. G. Russell, A. Nenes, Adjoint sensitivity of global cloud droplet number to aerosol and dynamical parameters. *Atmos. Chem. Phys.* **12**, 9041–9055 (2012).
42. T. Goren, D. Rosenfeld, Satellite observations of ship emission induced transitions from broken to closed cell marine stratocumulus over large areas. *J. Geophys. Res.* **117**, D17206 (2012).

Acknowledgments: We thank three anonymous reviewers for helpful and insightful comments. We also acknowledge the NASA student intern program. **Funding:** We acknowledge the following funding support: NASA grants 80NSSC18M0084 (to T.Y., H.S., R.W., K.M., and L.O.) and NNH20ZDA001N-TASNPP (to T.Y., H.S., C.W., K.M., L.O., and S.E.P.). **Author contributions:** Conceptualization: T.Y. Data analysis: T.Y., H.S., C.W., S.v.H., and S.L. Writing—original draft: T.Y. Writing—review and editing: R.W., C.W., L.O., S.E.P., K.M., S.v.H., S.L., and E.W. **Competing interests:** The authors declare that they have no competing interests. **Data and materials availability:** The native MODIS and MERRA-2 data are openly available at https://ladsweb.modaps.eosdis.nasa.gov/ and https://gmao.gsfc.nasa.gov/reanalysis/MERRA-2/. The ship-track density data used here are available at https://dataverse.harvard.edu/dataset.xhtml?persistentId=doi:10.7910/DVN/Q2LLJA. Location and time of each ship-track can be found at https://doi.org/10.7910/DVN/JII4DN. Our code is based on the model found at https://github.com/usuyama/pytorch-unet. All data needed to evaluate the conclusions in the paper are present in the paper and/or the Supplementary Materials.

Submitted 20 December 2021
Accepted 8 June 2022
Published 22 July 2022
10.1126/sciadv.abn7988

ScienceAdvances

Global reduction in ship-tracks from sulfur regulations for shipping fuel

Tianle Yuan, Hua Song, Robert Wood, Chenxi Wang, Lazaros Oreopoulos, Steven E. Platnick, Sophia von Hippel, Kerry Meyer, Siobhan Light, and Eric Wilcox

Sci. Adv., **8** (29), eabn7988.
DOI: 10.1126/sciadv.abn7988